

Temperature and length scale dependence of solvophobic solvation in a single-site water-like liquid

John R. Dowdle,¹ Sergey V. Buldyrev,² H. Eugene Stanley,³ Pablo G. Debenedetti,⁴ and Peter J. Rossky^{5,a)}

¹*The Dow Chemical Company, Freeport, Texas 77541, USA*

²*Department of Physics, Yeshiva University, New York, New York 10033, USA*

³*Center for Polymer Studies and Department of Physics, Boston University, Boston, Massachusetts 02215, USA*

⁴*Department of Chemical and Biological Engineering, Princeton University, Princeton, New Jersey 08544, USA*

⁵*Institute for Computational Engineering and Sciences and Department of Chemical Engineering, The University of Texas at Austin, Austin, Texas 78712, USA*

(Received 4 November 2012; accepted 17 January 2013; published online 12 February 2013)

The temperature and length scale dependence of solvation properties of spherical hard solvophobic solutes is investigated in the Jagla liquid, a simple liquid that consists of particles interacting via a spherically symmetric potential combining a hard core repulsion and a longer ranged soft core interaction, yet exhibits water-like anomalies. The results are compared with equivalent calculations for a model of a typical atomic liquid, the Lennard-Jones potential, and with predictions for hydrophobic solvation in water using the cavity equation of state and the extended simple point charge model. We find that the Jagla liquid captures the qualitative thermodynamic behavior of hydrophobic hydration as a function of temperature for both small and large length scale solutes. In particular, for both the Jagla liquid and water, we observe temperature-dependent enthalpy and entropy of solvation for all solute sizes as well as a negative solvation entropy for sufficiently small solutes at low temperature. This feature of water-like solvation is distinct from the strictly positive and temperature independent enthalpy and entropy of cavity solvation observed in the Lennard-Jones fluid. The results suggest that, compared to a simple liquid, it is the presence of a second thermally accessible repulsive energy scale, acting to increasingly favor larger separations for decreasing temperature, that is the essential characteristic of a liquid that favors low-density, open structures, and models hydrophobic hydration, and that it is the presence of this second energy scale that leads to the similarity in the behavior of water and the Jagla liquid. In addition, the Jagla liquid dewets surfaces of large radii of curvature less readily than the Lennard-Jones liquid, reflecting a greater flexibility or elasticity in the Jagla liquid structure than that of a typical liquid, a behavior also similar to that of water's hydrogen bonding network. The implications of the temperature and length scale dependence of solvation free energies in water-like liquids are explored with a simple model for the aggregation of solvophobic solutes. We show how aggregate stability depends upon the size of the aggregate and the size of its constituent solutes, and we relate this dependence to cold-induced destabilization phenomena such as the cold-induced denaturation of proteins. © 2013 American Institute of Physics. [<http://dx.doi.org/10.1063/1.4789981>]

I. INTRODUCTION

Among the many anomalous properties of liquid water is the solvation behavior of small apolar solutes, which is characterized at ambient conditions by an unfavorable entropy of transfer from vapor phase to water and an atypical decrease in solubility with increasing temperature. This behavior contrasts with typical solvents, which more readily accommodate apolar compounds as thermal fluctuations increase. The enthalpy of transfer for non-polar solutes to low-temperature water is actually negative and favorable, but the solubility is dominated by the entropic penalty. These characteristics change as a function of temperature and solute size. At sufficiently high temperatures the enthalpy is large and unfavorable and is only partially compensated for by favorable trans-

fer entropies. Similarly, for sufficiently large solutes, the poor solubility is dominated by the unfavorable enthalpy associated with the formation of an interface, which overcomes the favorable entropy gain.¹

Recent theoretical work in the field of hydrophobic solvation²⁻⁷ has refocused attention on the size-dependence of solvation free energy for small and large solutes, which is generally accepted to play a potentially important role in the formation and stabilization of many biological structures including proteins and cell membranes. Specifically, it was demonstrated that the solvation free energies of simple hard sphere solutes in water at ambient conditions undergo a crossover in size dependence at about 1 nm.¹ For solutes of size smaller than 1 nm, the solvation free energy scales with the volume of the solute, while for larger solutes it scales with the surface area. This crossover behavior is general to all

^{a)}Electronic mail: rossky@mail.utexas.edu.

liquids far from the critical point and near liquid-vapor coexistence, but the length scale of the crossover in water is greater than that of simple liquids, such as a simple Lennard-Jones (LJ) liquid.³ This longer crossover distance is attributed to water's propensity to create available space throughout its hydrogen bonding network.

Traditional explanations of hydrophobic behavior, and water-like anomalies in general, place emphasis on the orientational interactions of water molecules (hydrogen bonding) and the accompanying tendency for tetrahedral structure. However, it has been demonstrated^{8–10} that water-like thermodynamic and structural anomalies can also be manifested by a recently introduced family of spherically symmetric potentials which possess two characteristic length scales (the Jagla model^{11,12}), a hard core and a longer ranged soft core repulsion. Further, the Jagla model has also been shown to exhibit water-like solvation thermodynamics.^{13,14} In particular, the solubility of simple hard sphere solutes in the Jagla liquid is a non-monotonic function of the temperature, and furthermore, a polymer composed of such hard spheres exhibits a solvent-induced collapsed state with a stability diagram in the pressure-temperature plane reminiscent of that of a typical globular protein in water.^{13,15,16} These results confirm that orientational interactions are not necessary to produce these features of water-like solvation behavior^{17–19} and suggest that the presence of two competing length scales is a fundamental physical feature of hydrophobic hydration.

Questions still remain, however, about the similarities between solvation in the Jagla liquid and water. In particular, what are the energetic and entropic contributions to the solvation free energy in the Jagla liquid and are they similar to those of water? Over what length scales do the analogies in solvation behavior between the two liquids extend? Is the length scale crossover behavior in the Jagla liquid similar to that of other simple liquids, or does it also mimic that of water? In the present study, we address all of these questions using extensive Monte Carlo (MC) simulations of the Jagla liquid. In addition, we compare results for water and the Jagla liquid to results for the LJ liquid wherever possible. In doing so we clarify what is indeed unique to water-like solvation and what is common in typical liquids.

This paper is organized as follows. In Sec. II, we describe the theoretical and computational methods used to calculate the thermodynamic quantities of interest. In Sec. III, we describe the interparticle potentials used and the details of the simulation protocols. The results of the calculations are presented and discussed in Sec. IV, and conclusions and future directions are given in Sec. V.

II. THEORETICAL AND COMPUTATIONAL METHODS

All solvation properties of a solute may be obtained once the excess chemical potential is known. Thus, our calculations focus on the evaluation of the excess chemical potential of a cavity solute, μ_c^x , which is formally given by

$$\mu_c^x(R) = -k_B T \ln p_0(R), \quad (1)$$

where T is the temperature, k_B is Boltzmann's constant, and $p_0(R)$ is the probability of finding a cavity of size R or larger

around a randomly located point in solution. For sufficiently small cavities, $p_0(R)$ may be evaluated directly via the test particle insertion method.^{20,21} In dense liquids, however, the probability of observing density fluctuations extreme enough to accommodate cavities much larger than the solvent particles is exceedingly small, and test particle insertion is known to fail in this case.²²

There are several methods available for the evaluation of chemical potentials for large cavities (see, e.g., Ref. 23), but for the Jagla and LJ fluids in this study we choose to use the revised scaled particle theory (RSPT) of Ashbaugh and Pratt.^{24,25} Here we give only a brief overview of RSPT which closely follows that given in Ref. 26. For more detailed descriptions the reader is referred to Refs. 24 and 25.

RSPT improves upon classical scaled particle theory (SPT)^{27,28} by including multi-body correlations. The essential idea behind both RSPT and SPT is that the excess chemical potential must be equal to the work required to inflate a cavity against the solvent from size zero to R . This work must oppose the pressure due to the solvent molecules at the cavity boundary, and thus scaled particle theories require knowledge of the contact correlation function, $G(R)$, defined to be the average density of solvent molecules, relative to the bulk, at the cavity-solvent interface. With $G(R)$ known, the excess chemical potential is calculated as

$$\mu_c^x(R) = \int_0^R k_B T \rho G(r) 4\pi r^2 dr, \quad (2)$$

where ρ is the bulk solvent number density. For R much greater than the solvent size, the contact correlation function may be expanded in curvature, R^{-1} , with phenomenological coefficients

$$G(R) = \frac{\beta P}{\rho} + \frac{2\beta\gamma_\infty}{\rho R} - \frac{4\beta\gamma_\infty\delta}{\rho R^2} + \dots \quad (3)$$

Here, P is the bulk pressure, γ_∞ is the surface tension of a flat solvent-cavity interface, and δ is the first-order curvature correction to the surface tension.²⁶ An expression for the excess chemical potential of large cavity solutes is then obtained by expanding Eq. (3) to fourth order and integrating to get

$$\begin{aligned} \mu_c^x(R)|_{\text{large}} = & \frac{4\pi R^3 P}{3} + 4\pi R^2 \gamma_\infty - 16\pi \gamma_\infty \delta R \\ & + 4\pi k_B T \rho \kappa - \frac{4\pi k_B T \rho \lambda}{R}, \end{aligned} \quad (4)$$

where λ is the fourth-order curvature correction coefficient and κ is an integration constant. Third order coefficients are typically set to zero so as to avoid logarithmic contributions to μ_c^x ,^{29,30} a convention we follow in this work. The results for the test particle insertion calculations for small cavities, $\mu_c^x(R)|_{\text{sim}}$, are interpolated with the large cavity solute expression in Eq. (4) by

$$\mu_c^x(R) = \mu_c^x(R)|_{\text{sim}} f(R) + \mu_c^x(R)|_{\text{large}} (1 - f(R)). \quad (5)$$

The function $f(R)$ used here is a cubic function designed to smoothly switch between small (R_{sim}) and large (R_{large})

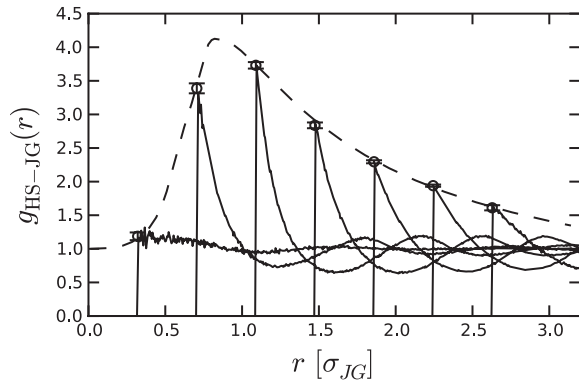


FIG. 1. Demonstration of a fit of Eq. (7) for the cavity contact correlation function to calculated contact values for several cavity sizes in the Jagla liquid at $T = 0.6$ [ε_2/k_B]. The contact correlation function, $G(R)$ (dashed line), is fit to the maxima (open circles) in the cavity-solvent pair correlation functions, $g_{HS-JG}(r)$ (solid lines). The cavity radii are, in units of σ_{JG} , 0.32, 0.71, 1.09, 1.47, 1.86, 2.24, and 2.63.

cavity sizes,

$$f(R) = \begin{cases} 1, & R < R_{\text{sim}}, \\ 1 - 3 \frac{(R - R_{\text{sim}})^2}{(R_{\text{large}} - R_{\text{sim}})^2} + 2 \frac{(R - R_{\text{sim}})^3}{(R_{\text{large}} - R_{\text{sim}})^3}, & R_{\text{sim}} \leq R \leq R_{\text{large}}, \\ 0, & R > R_{\text{large}}. \end{cases} \quad (6)$$

In order to obtain parameters appearing in the expansion for the contact correlation function, we use Eq. (5) and differentiate Eq. (2) with respect to R to obtain the contact correlation function as

$$G(R) = \frac{f(R)}{4\pi\rho R^2} \frac{\partial \beta \mu_c^x(R)|_{\text{sim}}}{\partial R} + \frac{\beta \mu_c^x(R)|_{\text{sim}}}{4\pi\rho R^2} \frac{\partial f(R)}{\partial R} + \left(\frac{\beta P}{\rho} + \frac{2\beta\gamma_\infty}{\rho R} - \frac{4\beta\gamma_\infty\delta}{\rho R^2} + \frac{\lambda}{R^4} \right) [1 - f(R)] - \left(\frac{\beta P R}{3\rho} + \frac{\beta\gamma_\infty}{\rho} - \frac{4\beta\gamma_\infty\delta}{\rho R} + \frac{\kappa}{R^2} - \frac{\lambda}{R^3} \right) \frac{\partial f(R)}{\partial R} \quad (7)$$

and fit this function to the contact values calculated from the MC simulations, as demonstrated in Fig. 1. The pressure is set equal to the simulation pressure, and the parameters γ_∞ , δ , κ , and λ are fit to the simulation results.

The contact density calculations for the Jagla and LJ liquids demand significant amounts of computer time to obtain good statistics, and performing similar calculations for typical multi-site water models that have electrostatic interactions is not desirable. For our purposes of comparison here, we may, however, estimate the excess chemical potential of large cavities in water over a broad range of thermodynamic states by using the recently developed cavity equation of state (C-EoS).³¹ The C-EoS is an analytical equation of state parameterized to fit experimental and simulation results for water, and it has been shown to accurately reproduce hydrophobic solvation thermodynamics of simple hydrophobes when combined with a first-order perturbation theory. The functional form of the C-EoS is given by

$$\beta \mu_c^x = a + b\beta + c \ln \beta, \quad (8)$$

where μ_c^x is the cavity chemical potential and the coefficients, a , b , and c are assumed to be temperature independent. Thus, the C-EoS assumes that the enthalpy of cavity formation depends linearly upon temperature and that the associated heat capacity is temperature independent. The dependence of μ_c^x on the cavity size, R , is obtained by expanding in powers of $1/R$ and requiring that $\beta \mu_c^x$ approach $\gamma_{lv} a_0$ in the large cavity limit, where γ_{lv} is the experimental liquid-vapor surface tension and $a_0 = 4\pi R^2$ is the cavity surface area,

$$\beta \mu_c^x / a_0 = \sum_{i=0}^3 A_i (1/R)^i + \left[\sum_{i=0}^3 B_i (1/R)^i \right] \beta + \left[\sum_{i=0}^3 C_i (1/R)^i \right] \ln \beta. \quad (9)$$

The remaining coefficients A_i , B_i , and C_i are obtained from fits to simulation data.

III. SIMULATION DETAILS

MC simulations of cavity solvation in the Jagla and LJ fluids were performed along the liquid vapor coexistence curves of each liquid for states ranging from the triple point to slightly below the critical point. The Jagla potential is given by

$$u_{JG}(r) = \begin{cases} \infty, & r < r_0, \\ m_1 r + b_1, & r_0 < r \leq r_1, \\ m_2 r + b_2, & r_1 < r \leq r_2, \\ 0, & r > r_2, \end{cases} \quad (10)$$

where

$$m_1 = \frac{-(\varepsilon_2 + \varepsilon_1)}{r_1 - r_0}, \quad (11)$$

$$b_1 = -\varepsilon_2 - m_1 r_1, \quad (12)$$

$$m_2 = \frac{\varepsilon_2}{r_2 - r_1}, \quad (13)$$

$$b_2 = -\varepsilon_2 - m_2 r_1. \quad (14)$$

This potential, shown in Fig. 2, demonstrates a wide range of behavior for varying parameters, including limiting cases of hard sphere, triangle well, and ramp potentials. Here we choose $r_1 = 1.72r_0$, $r_2 = 3.0r_0$, and $\varepsilon_1 = 3.5\varepsilon_2$, as this particular parameterization manifests a cascade of water-like anomalies.^{9,13,32,33}

For the LJ fluid we use the cut-shifted LJ interaction given by

$$u_{LJ}^{\text{cut}}(r) = \begin{cases} u_{LJ}(r) - u_{LJ}(r_c), & r < r_c, \\ 0, & r \geq r_c, \end{cases} \quad (15)$$

where $u_{LJ}(r) = 4\varepsilon_{LJ} (\sigma_{LJ}^{12}/r^{12} - \sigma_{LJ}^6/r^6)$ is the full LJ interaction, ε_{LJ} and σ_{LJ} are the well depth and solvent diameter, respectively, and the cutoff distance, r_c , used is chosen as $2.5\sigma_{LJ}$.

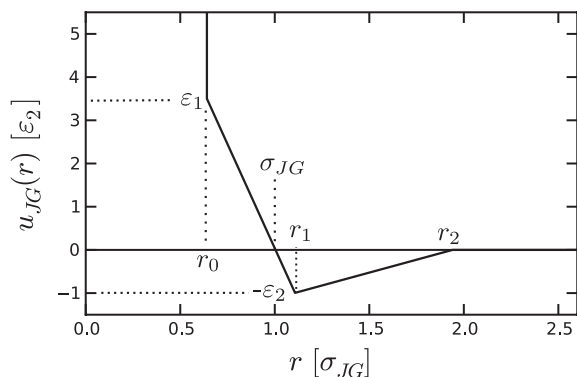


FIG. 2. The Jagla two-ramp potential. The parameters used in the present studies are the same as in Ref. 13, viz.: $r_1 = 1.72r_0$, $r_2 = 3.0r_0$, and $\epsilon_1 = 3.5\epsilon_2$. The relative values of the hard core (r_0) and the soft core (r_1) positions roughly correspond to the same ratio between the positions of the first and second solvation shells of liquid water. The effective size of the Jagla particle, σ_{JG} , is estimated from plots of the radial distribution to be the minimum separation at which $u_{JG}(r) = 0$ (see Fig. 3).

Several different sets of Monte Carlo simulations were performed on the Jagla liquid. In the first, saturation properties of the Jagla fluid were estimated from canonical ensemble MC simulations of a liquid slab in equilibrium with its vapor for selected temperatures ranging from near the triple point to just below the critical point. From these slab simulations we estimate saturated liquid and vapor densities, the saturation pressure, and the liquid-vapor surface tension along the binodal line. The surface tension, γ_{lv} , is calculated from the profiles of the pressure tensor using the mechanical definition.^{34,35} The results for the saturation properties are shown in Table I.

In the second set of simulations, isothermal-isobaric MC simulations of the Jagla fluid were performed for both the liquid and vapor phases at each of the saturation states listed in Table S1 in the supplementary material.³⁶ Test particle insertion calculations were performed on the resulting liquid phase trajectories for cavities up to $2\sigma_{JG}$ in diameter to obtain $\mu_c^x(R)|_{\text{sim}}$. Similarly, insertion probabilities and excess chemical potentials for cavities up to $6\sigma_{JG}$ in diameter were obtained from test particle insertion analysis of the vapor phase

TABLE I. Canonical ensemble MC simulations of a liquid slab in equilibrium with its vapor were performed to obtain estimates of saturation properties. N Jagla particles were simulated at five different temperatures for 1.6×10^6 MC cycles, where one cycle corresponds to N MC moves. The liquid and vapor densities were estimated from ensemble averages of the densities in the centers of the liquid and vapor regions, respectively. Similarly, the saturation pressure was obtained by evaluating the pressure tensor in the center of the vapor region. The liquid-vapor surface tension is calculated using the virial relation.^{34,35} Numbers in parentheses are estimates of the statistical error in the last digit of the reported value.

N	T [ϵ_2/k_B]	ρ_l [r_0^{-3}]	ρ_v [r_0^{-3}]	P_{sat} [ϵ_2/r_0^3]	γ_{lv} [ϵ_2/r_0^2]
1374	0.4	0.256(2)	$5(3) \times 10^{-5}$	$3(2) \times 10^{-5}$	0.491(8)
1374	0.6	0.255(2)	$2.3(7) \times 10^{-4}$	$1.4(4) \times 10^{-4}$	0.407(7)
1386	0.8	0.244(2)	0.0018(2)	0.0014(2)	0.314(8)
1444	1.0	0.226(3)	0.0067(6)	0.0056(6)	0.213(5)
1600	1.2	0.203(2)	0.0174(9)	0.015(1)	0.115(7)

trajectories. Knowledge of the vapor phase chemical potentials allows evaluation of the surface tension at the vapor wall interface.²⁶

Finally, isothermal-isobaric MC simulations of a single cavity in the Jagla liquid were performed for various cavity sizes at each of the saturation states listed in Table S1 in the supplementary material.³⁶ Cavity diameters up to $6\sigma_{JG}$ were considered, and the contact correlation function was evaluated for each cavity at each state point. The contact correlation function is determined by extrapolating the cavity-solvent pair correlation function to contact.

The parameters in Eq. (7) may be fit to the MC results for $G(R)$, and the cavity excess chemical potential may then be computed from Eq. (5). The details of the MC simulations used to calculate the insertion probabilities and contact correlation functions in the Jagla fluid are provided in Tables S1 and S2 in the supplementary material.³⁶ All data for the LJ liquid are those obtained in the studies reported in Ref. 26. The saturation states for the LJ liquid are also listed in Table S4 in the supplementary material³⁶ for the present study.

Molecular dynamics simulations of the extended simple point charge (SPC/E) water model³⁷ were performed along the liquid vapor coexistence curve for each of the states listed in Table S5 in the supplementary material.³⁶ A system consisting of 512 SPC/E water molecules was simulated in a cubic box with periodic boundary conditions in the canonical ensemble for 20 ns using the GROMACS molecular dynamics engine.^{38,39} The time step was chosen as 2 fs, and bonds were constrained with the SETTLE algorithm.⁴⁰ The velocity rescaling thermostat was used to control temperature with a time constant of 0.1 ps.⁴¹ Particle mesh Ewald summation was used to treat long range electrostatic interactions⁴² with a real space cutoff of 1.2 nm and a mesh spacing of 0.18 nm. The Ewald tolerance was set to 10^{-5} , and fourth order interpolation was used.

IV. RESULTS AND DISCUSSION

A. The definition of solvent size from pair distribution functions

A comparison of the solvent-solvent pair correlation function, $g(r)$, for the three liquids is shown in Fig. 3. The maximum in $g(r)$ for the LJ liquid occurs at a pair separation slightly larger than σ_{LJ} , and at a separation of σ_{LJ} the pair distribution function assumes a value of very nearly one for all states on the saturation curve. The nearest separation at which $g(r)$ is unity is a commonly used estimate for the size of a particle since the surrounding fluid is depleted from all shorter distances. We adopt this estimate here and use σ_{LJ} as the size of the LJ particle.

In the case of SPC/E water, the pair distribution function peaks at about 0.28 nm at ambient temperature and slightly larger distances at higher temperatures. These distances are smaller than the LJ diameter for oxygen due to H-bonding. The nearest separation at which $g(r)$ is unity is nearly constant at about 0.26 nm, which, to be consistent, is our choice for the size of the SPC/E molecule, σ_{Wat} .

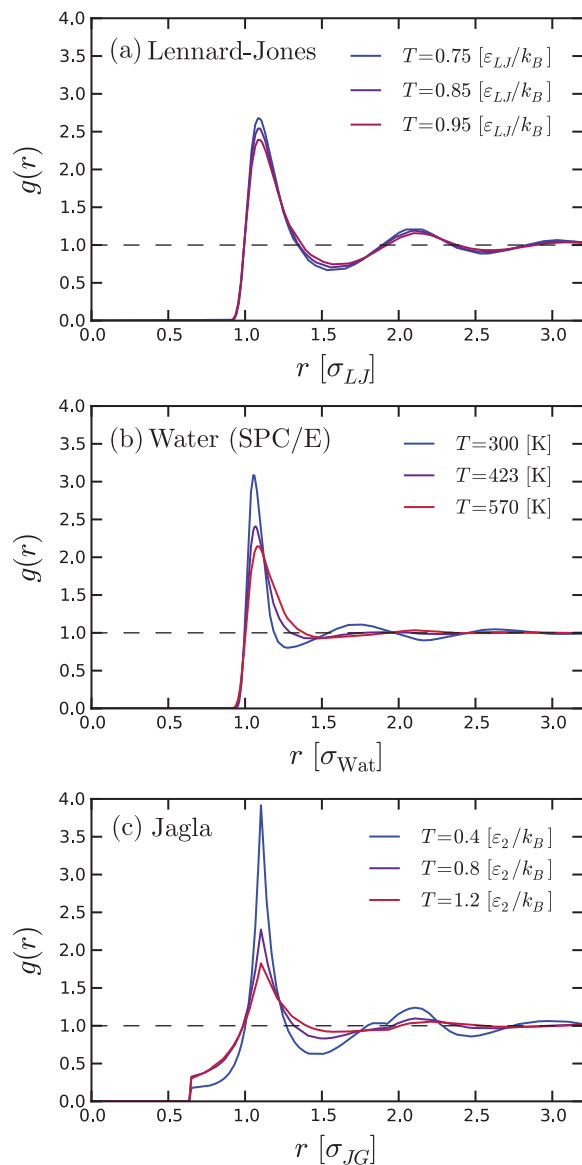


FIG. 3. Solvent-solvent pair distribution functions for states along the saturation curves of (a) the LJ liquid, (b) SPC/E water, and (c) the Jagla liquid. It is evident from the figure that the minimum separation at which $g(r)$ has the value unity can be used as an estimate for the solvent size. For the SPC/E model this corresponds to $\sigma_{\text{Wat}} = 0.26$ nm, for the LJ liquid it is σ_{LJ} , and for the Jagla liquid it is $\sigma_{\text{JG}} = 1.56r_0$ (the minimum separation at which $u_{\text{JG}}(r) = 0$). These sizes are taken to be independent of temperature for the states considered here, as justified by the data shown.

The maximum peak in the Jagla liquid $g(r)$ occurs at a distance significantly larger than the hard core diameter, r_0 . This reflects the preference of Jagla particles to maintain separation at the minimum in $u_{\text{JG}}(r)$, r_1 , unless stressed by temperature or pressure. This preference is diminished as temperature increases. However, the minimum separation at which the Jagla $g(r)$ is unity is found to be insensitive to temperature [see Fig. 3(c)] and closely corresponds to the minimum separation at which the pair potential is zero. This distance, σ_{JG} , is a consistent estimate for the size of the Jagla particle; $\sigma_{\text{JG}} = 1.56r_0$ for the potential parameterization considered here.

B. Surface tension and vapor-liquid equilibria in the Jagla fluid

In the first set of MC simulations, saturation properties of the Jagla fluid were estimated from canonical ensemble MC simulations of a liquid slab in equilibrium with its vapor for selected temperatures ranging from near the triple point to below the critical point. From these simulations we estimate liquid and vapor densities, the saturation pressure, and the liquid-vapor surface tension along the binodal line.

The results for the liquid-vapor slab simulations of the Jagla fluid are summarized in Table I. The saturated liquid densities and the equilibrium vapor densities are in close agreement with those reported by Lomba *et al.*⁴³ We expect that our estimates of the coexistence properties of the Jagla fluid may be improved upon by taking finite size effects into account, as it is known, e.g., that large wavelength fluctuations may be suppressed by the system size.⁴⁴ Nevertheless, the solvation behavior we seek to characterize occurs for states at or near coexistence,³ and we therefore expect the present estimates from the slab simulations to suffice for this study.

C. Cavity solvation thermodynamics

The parameters in Eq. (7) were fit to the MC results for $G(R)$ in the Jagla liquid using a least-squares regression. The choice of R_{sim} and R_{large} used in the fit varied with the thermodynamic state. Values of R_{sim} ranged from 0.5 to $0.6\sigma_{\text{JG}}$ and values of R_{large} ranged from 0.75 to $0.95\sigma_{\text{JG}}$. In all cases, $G(R)$ was well represented between R_{sim} and R_{large} by differentiation of $\mu_c^x(R)|_{\text{sim}}$. The results of the fit are presented in Table II. The surface tension of the flat interface, γ_∞ , is higher than the liquid-vapor surface tension measured in the slab simulations at all temperatures, as seen in Fig. 4(a). It should be emphasized that γ_∞ does not strictly correspond to the liquid-vapor surface tension, but rather to the total interfacial free energy between the solvent and the cavity which consists of contributions from two interfaces—a liquid vapor interface between the solvent and vapor film surrounding the cavity and the vapor-wall interface between the vapor film and the cavity surface. If the two interfaces are well separated and not interacting with one another, then γ_∞ is equal to the sum of the liquid-vapor and vapor-wall surface tensions. Our

TABLE II. Parameters from the least-squares fit of Eq. (7) to the contact densities obtained from the simulations in Table S2 in the supplementary material.³⁶ The simulation data were split into several blocks, and the numbers in parentheses represent an error in the last digit in the fitted parameter corresponding to one standard deviation of the block averages.

T [ϵ_2/k_B]	γ_∞ [ϵ_2/r_0^2]	δ [r_0]	κ [r_0^3]	λ [r_0^4]
0.4	0.55(1)	-0.01(2)	-13.2(5)	-8.1(9)
0.5	0.51(1)	-0.09(3)	-11.4(5)	-6.6(7)
0.6	0.47(1)	-0.18(3)	-10.2(3)	-5.5(4)
0.7	0.43(1)	-0.27(4)	-9.3(2)	-4.8(4)
0.8	0.38(1)	-0.35(5)	-8.1(4)	-4.0(4)
0.9	0.33(2)	-0.45(5)	-7.2(2)	-3.4(5)
1.0	0.28(1)	-0.59(6)	-6.5(1)	-2.9(6)
1.1	0.22(2)	-0.77(5)	-5.8(1)	-2.5(4)
1.2	0.17(2)	-0.93(5)	-4.8(1)	-1.9(2)

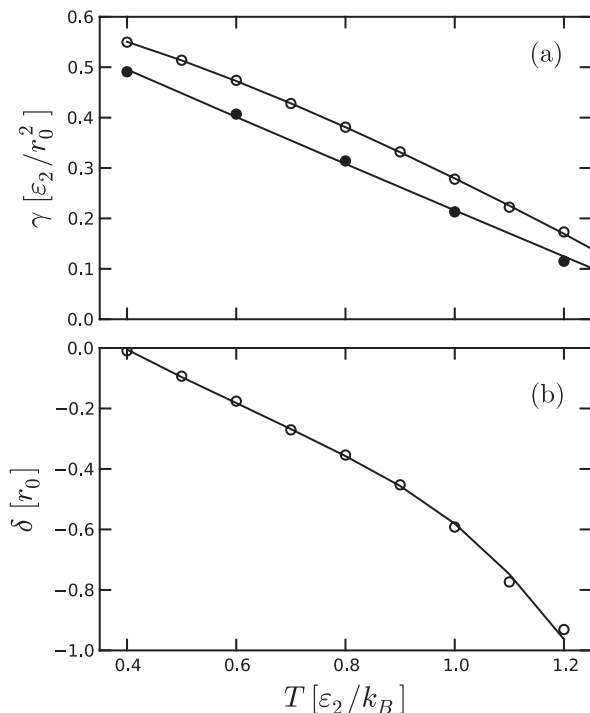


FIG. 4. Simulation results for the (a) interfacial free energy and (b) first order curvature correction as a function of temperature along the saturation curve of the Jagla fluid. The filled circles in (a) are the results for γ_{lv} , the liquid-vapor surface tension, while the open circles are the results for γ_{∞} , the interfacial free energy between the fluid and a hard wall (see text). Both γ_{∞} and δ are obtained through fits of Eq. (7) to MC simulation data. Statistical errors are smaller than symbol size. The lines in (a) are fits of the γ_{∞} and γ_{lv} data to Eq. (18), while the line in (b) is obtained from a fit of the product $\gamma_{\infty}\delta$ to Eq. (18). The parameters for the fits are given in Table S8 in the supplementary material.³⁶

simulations are sufficiently far from the critical point that the vapor-wall surface tensions are negligible for all states considered. Furthermore, the fitted values of γ_{∞} were insensitive to varying the maximum cavity diameter used in the fits between $4\sigma_{JG}$ and $6\sigma_{JG}$, suggesting the finite cavity sizes considered here are not to blame. Therefore, the difference between γ_{∞} and γ_{lv} is likely due to other factors such as the finite-size limitations of our estimates of γ_{lv} or the physical impact of quenched fluctuations at the solvent-wall interface.²⁶

The first order curvature correction to the surface tension, δ , has a long history in the discussion of length scale effects on solvation dating back to Tolman's original article.⁴⁵ It was pointed out by Huang and Chandler⁴⁶ and demonstrated by Graziano⁴⁷ that when δ is treated as temperature-independent, the cavity hydration entropy does not change sign with increasing solute size. More recently, using a temperature-dependent δ Ashbaugh⁴⁸ derived an expression for the cavity size at which the solvation entropy changes sign from negative to positive and demonstrated the fidelity of its predictions along the saturation curves of water and *n*-hexane. We choose here to treat δ as a temperature-dependent fitting parameter. The results of our fit [Table II and Fig. 4(b)] show that δ is negative for all states considered and decreases with increasing temperature, consistent with results for the LJ liquid²⁶ and recent results for the SPC/E water model.⁴⁹ The parameters κ and λ are negative for all states and diminish in magnitude as the critical point is approached.

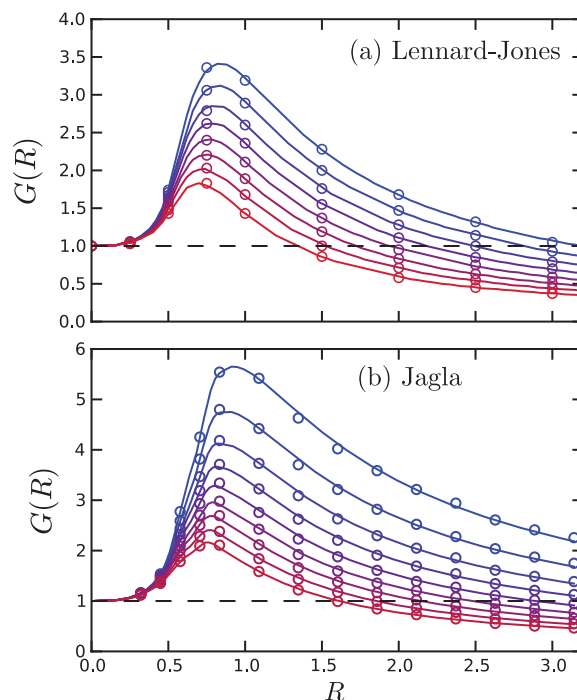


FIG. 5. Cavity contact correlation functions as a function of cavity size (measured in units of solvent diameters) for states along the saturation curves of the (a) LJ and (b) Jagla liquids ranging from near the triple point (blue) to just below the critical point (red). The temperatures for the LJ liquid range from $k_B T/\epsilon_{LJ} = 0.65$ (blue) to 1.00 (red) in increments of 0.05, while those for the Jagla liquid range from $k_B T/\epsilon_2 = 0.4$ (blue) to 1.2 (red) in increments of 0.1. Points are obtained from MC simulation data and lines are fits of Eq. (7) to the simulation data. Statistical errors are smaller than symbol size. All LJ data are obtained from Ref. 26.

The results of the MC calculations for the cavity contact correlation functions are shown in Fig. 5 along with the fits to $G(R)$. In both fluids, as the solute size grows from zero, the solvent packs increasingly tightly until the contact density peaks at a value of R on the order of the solvent size. At this point, the solvent begins to pull away from the solute, and for sufficiently large solutes, $G(R)$ will be less than one. The contact correlation function is a decreasing function of temperature for all solute sizes studied here, but for sufficiently large solute sizes $G(R)$ will increase with temperature since $\lim_{R \rightarrow \infty} G(R) = \beta P/\rho$, which increases with temperature along the saturation curve.

The cavity sizes where $G(R)$ decreases below one, i.e., where the cavity is “dewet,” are larger relative to the solvent size in the Jagla liquid, meaning that the Jagla liquid resists dewetting of hard surfaces more than the LJ liquid. Finally, for a fixed cavity size in the LJ liquid the spacing in $G(R)$ values between temperatures appears roughly constant, suggesting a linear dependence upon temperature. This is not the case in the Jagla liquid, however, as the temperature dependence clearly decreases with increasing temperature.

With the fitted parameters for $G(R)$, the excess chemical potentials for the Jagla and LJ liquids may be obtained from Eq. (5). In the case of water we use Eq. (9). The results of the chemical potential calculations are shown in Fig. 6. The excess chemical potential is a positive, monotonically

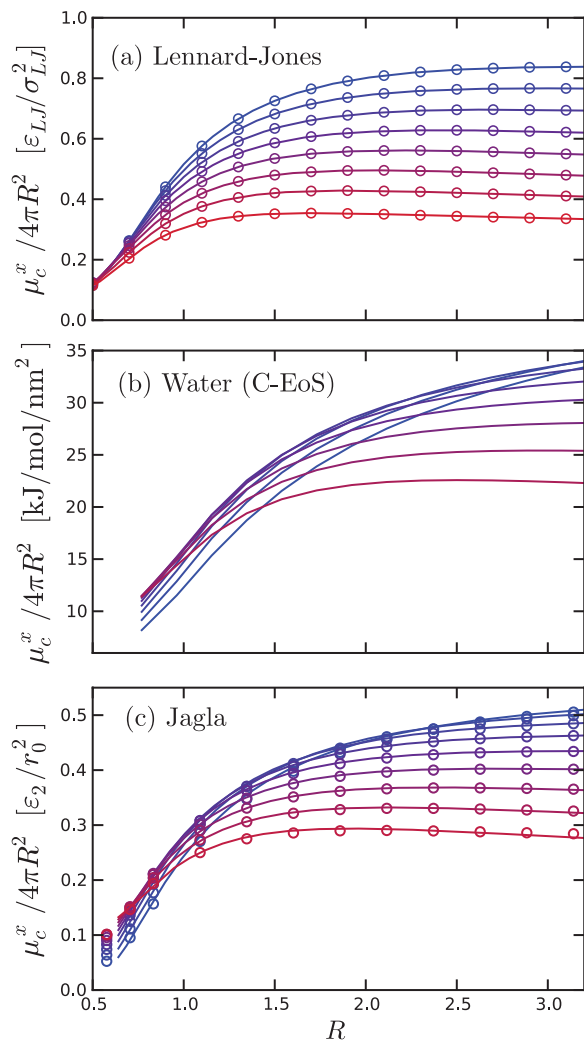


FIG. 6. Excess chemical potential per surface area versus cavity size (measured in units of solvent diameters) for states along the saturation curves of (a) the LJ liquid, (b) water, and (c) the Jagla liquid. The thermodynamic states for the LJ and Jagla liquids are the same as those presented in Fig. 5. Points in the Jagla and LJ plots are obtained from simulation data and scaled particle theory. Lines in the LJ plot are fits using Eq. (16), while lines in the Jagla plot are fits of the simulation data to the C-EoS [Eq. (9)]. Lines in (b) are predictions from the water C-EoS.³¹ The temperatures used for the water C-EoS plot are T [K] = 273, 304, 335, 366, 398, 429, 460, 491, and 522.

increasing function of cavity size at all temperatures in all three liquids.

In the LJ liquid, the chemical potential is a decreasing function of temperature for all cavity sizes greater than $\sigma_{LJ}/2$. Furthermore, the spacing between temperatures for any fixed cavity size appears roughly constant in the LJ liquid, which, as pointed out by Ashbaugh,²⁶ suggests that along the saturation curve the excess chemical potential may be modeled as

$$\mu_c^x(R) = h_c^x(R)|_\sigma - T s_c^x(R)|_\sigma, \quad (16)$$

where $h_c^x(R)|_\sigma$ and $s_c^x(R)|_\sigma$ are the temperature independent enthalpy and entropy of solvation. The enthalpy is positive and increases with cavity size, indicating the loss of favorable solvent-solvent interactions near the cavity solute. Except for cavities smaller than $\sigma_{LJ}/2$, the entropy is also a positive, increasing function of cavity size, indicating that solvent molecules near the cavity experience a net gain in configu-

rational space. The excellent fit of Eq. (16) to the simulation data [Fig. 6(a)], indicates that the enthalpy of solvation is approximately temperature-independent, and therefore the heat capacity of cavity solvation in the LJ liquid is approximately zero. In the Jagla liquid, in contrast, the chemical potential is an increasing function of temperature for small, solvent-sized cavities and a decreasing function of temperature for large cavities. The temperature derivative of the excess chemical potential for a fixed cavity size is not constant [Fig. 6(b)], but is evidently nonlinear. The qualitative behavior of the chemical potential of cavity solvation in the Jagla liquid is remarkably similar to that predicted for liquid water by the C-EoS. This suggests that the Jagla liquid data may be fit to the C-EoS as well. Using the surface tension data (Table I) and a least-squares fit of the excess chemical potentials calculated from the $G(R)$ data, we obtained a set of C-EoS parameters for the Jagla liquid (see Table S5). The fit is, in fact, excellent for all cavity sizes and temperatures considered, with slight deviations occurring only for the largest cavities at the highest temperature. The C-EoS fit to the simulation data permits exploration of the thermodynamic contributions to μ_c^x in the Jagla liquid using analytical derivatives of Eq. (9).

The enthalpic and entropic contributions to the excess chemical potential for the Jagla liquid and water may be obtained from analytical temperature derivatives of the C-EoS.^{54,55} The enthalpy and entropy of cavity solvation are compared in Fig. 7. The most obvious distinction between the three liquids is that the LJ liquid has temperature independent enthalpic and entropic contributions to the solvation free energy, while the contributions for the Jagla liquid and water both show a strong temperature dependence. For all three fluids, the enthalpy is a positive, monotonically increasing function of the cavity radius. The unfavorable enthalpy results from the disruption of the liquid structure in the vicinity of the solute and the concomitant formation of an interface which on average has fewer favorable solvent-solvent interactions than an equivalent volume in the bulk.

For any fixed cavity size in the size ranges considered in this study, the enthalpy is an increasing function of temperature in the Jagla liquid and in water which results in a positive heat capacity increment for cavity formation, a well-known signature of hydrophobic hydration. The calculated values for both liquids are provided graphically in the supplementary material.³⁶ A possible interpretation for this result in water is given by the Muller model,^{50,51} which uses a simple two-state hydrogen bond (H-bond) model parameterized by empirical solvation data to argue that the fraction of broken H-bonds in the solvation shell of apolar solutes is always at least somewhat greater than that in the bulk, and furthermore, that this disparity increases with temperature. Thus, for a fixed cavity size an increase in temperature decreases the number of H-bonds in the solvation shell relative to the bulk, which leads to a greater enthalpy.

The entropy of cavity formation in both the Jagla liquid and water increases with increasing temperature for any fixed cavity size. It is possible that this behavior in water may also be connected to the breaking of solvation shell H-bonds. If an increase in temperature causes a decrease in the number of solvation shell H-bonded pairs relative to bulk, then

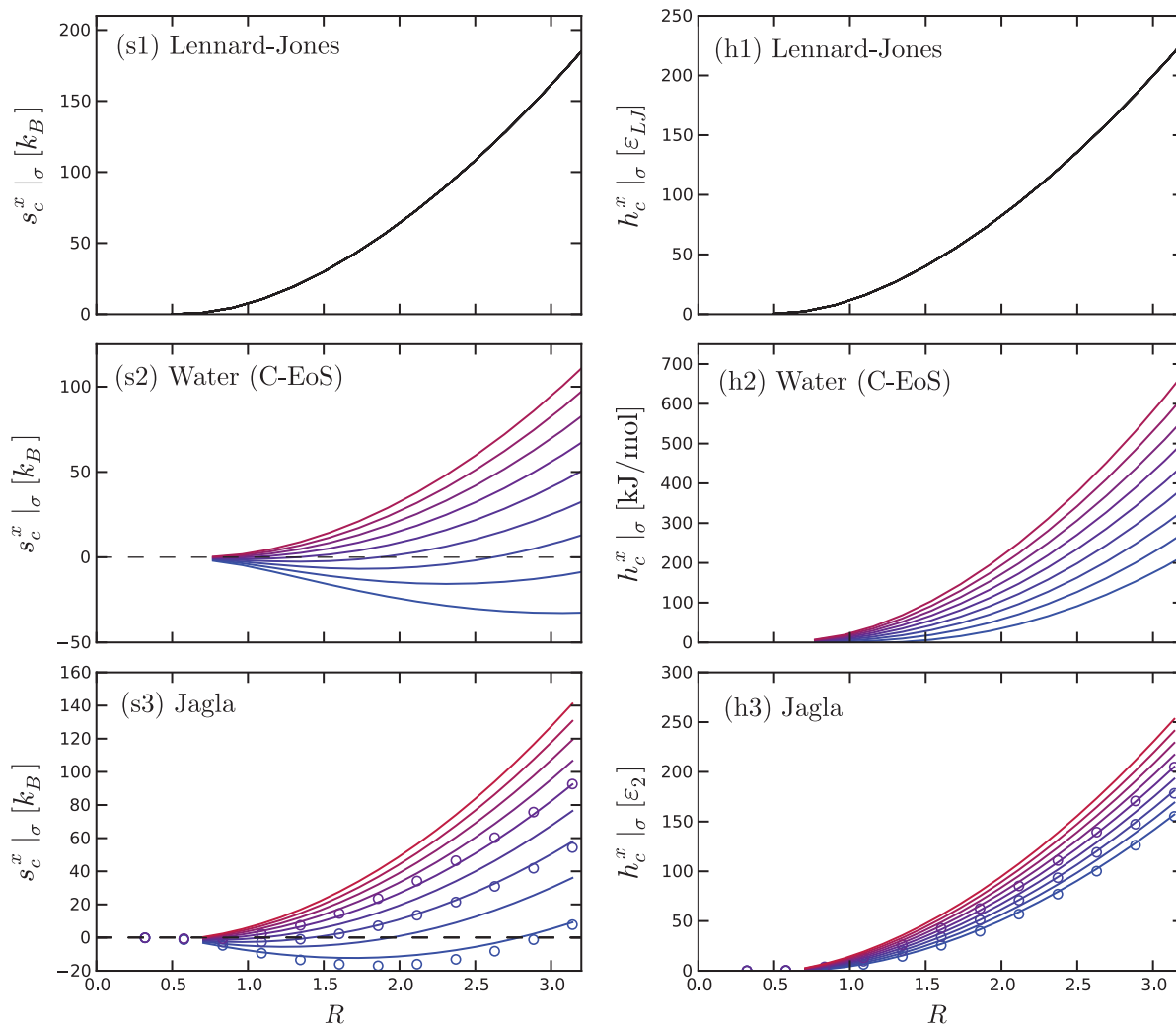


FIG. 7. (s1)–(s3) Entropy and (h1)–(h3) enthalpy of cavity solvation for the LJ liquid, water, and the Jagla liquid as a function of cavity size (measured in units of solvent diameters). The temperatures for the Jagla liquid are the same as those listed in Fig. 5, while the temperatures for the water C-EoS are the same as those listed in Fig. 6. For water and the Jagla liquid, entropies are calculated from temperature derivatives of the cavity equation of state (lines), $s_c^x |_\sigma = -(\partial \mu_c^x / \partial T)_\sigma$, while for the LJ liquid, the entropy is given by the assumed temperature-independent form of μ_c^x in Eq. (16). The enthalpy is calculated from $h_c^x |_\sigma = \mu_c^x + T s_c^x |_\sigma$. Points in (s3) and (h3) are numerical derivatives of cubic spline fits to the excess chemical potentials in Fig. 6.

overall the gain in configurational freedom will be larger at the higher temperature. However, this does not yet explain the Jagla model behavior.

It is remarkable that the Jagla liquid, which contains no orientational dependence in its interaction potential and therefore no H-bonding, reproduces the qualitative behavior of hydrophobic hydration thermodynamics. The underlying physical origins for this behavior in the Jagla liquid may be analogous to those of water, however. It has been shown in computer simulations of SPC/E water that the energetics of H-bonding are strongly correlated with local crowding effects. In particular, H-bonded pairs with a small number of neighbors will on average have a stronger H-bond than bonded pairs with a greater number of neighbors.⁵² Furthermore, the fraction of H-bonded pairs in interfacial regions of apolar moieties is lower than in the bulk liquid, and the bonded pairs that do exist in these regions tend to have fewer neighbors and stronger bonds than the average H-bonded pair in the bulk. The interpretation is that density fluctuations that create cavities select against weak H-bonds, leaving only the

stronger bonds to survive. Thus, the interfacial region experiences less H-bonding on the whole than equivalent volumes in the bulk, but maintains on average stronger hydrogen bonds.

A plausible analogy in the Jagla liquid to H-bonding in water is the interaction of particle pairs at the potential minimum distance, r_1 . As temperature is lowered, the liquid prefers to adopt configurations that maximize the number of particle pairs near a separation of r_1 , which in the limit of the crystal is a hcp lattice.³³ This is analogous to water maximizing the number of H-bonded pairs at low temperatures by adopting a tetrahedral network structure, and thus the Jagla pair interactions near r_1 become analogous to water's H-bond. Under this view, density fluctuations in the Jagla liquid disrupt weakly interacting Jagla particles and leave a solvation shell that consists of fewer pair interactions near r_1 . The fraction of “broken” interactions at r_1 in the solvation shell would increase faster with temperature than the same quantity in the bulk. Future work entailing a detailed analysis of solvation shell structure will be needed to demonstrate if this hypothesis is correct.

The LJ liquid demonstrates enthalpic and entropic behaviors in sharp contrast to those of water and the Jagla liquid. The entropy is strictly positive for all cavities of size $R > 0.5\sigma_{LJ}$ in the LJ liquid, and the heat capacity increment is negligible. This latter phenomenon is consistent with the argument for the temperature dependence of the relative fraction of broken H-bonds in solvation shell water compared to bulk water—i.e., the absence of a second energy scale in the LJ liquid precludes a temperature-dependent enthalpy of cavity formation analogous to that of water. This implies that the fundamental commonality between water and Jagla fluids is the presence of two energy scales, each coupled to a different length scale, so that low density, open structures are increasingly favored for decreasing temperature, the feature absent in simple liquids. In the Jagla model, the second energy and length scale is set by the ratios describing the soft ramp, ϵ_1/ϵ_2 and r_1/r_0 , while in water, these are determined by characteristics of the H-bonded and non-H-bonded states.

D. The length scale crossover

As seen in Fig. 6, the chemical potential decreases with temperature along the coexistence curve for all cavity sizes considered in the LJ liquid. However, in water and the Jagla liquid, the chemical potential increases with increasing temperature for solvent-sized cavities and decreases with temperature for larger cavities. Qualitatively, the temperature dependence of the solvation free energy is identical in the Jagla liquid and water.

An important consequence of the similarities between the temperature-dependence of the solvation free energies in the Jagla liquid and water is that the water-like characteristic of negative solvation entropy for small cavities is observed in the Jagla liquid (Fig. 7). As the cavity size increases from $R = 0.5\sigma_{JG}$, the curves along each saturation state first decrease, then pass through a minimum before increasing monotonically for larger cavities. For cavities large enough that $s_c^x|_\sigma > 0$, the solvation shell is more disordered, and for sufficiently large cavities a dewetting transition will occur. This “entropic crossover” from negative to positive solvation entropy may therefore be viewed as a measure of the length scale at which interface formation begins to dominate the solvation free energy. In this view, the crossover for the LJ liquid occurs at cavity sizes less than σ_{LJ} in diameter for all saturation states, which is smaller than the smallest cavities explicitly studied here. In water and the Jagla liquid however, the entropic crossover distance predicted by the C-EoS grows many times larger than the solvent diameter as temperature is decreased, as shown in Fig. 8. Also shown in Fig. 8 are predictions from Ashbaugh’s expression for the crossover radius⁴⁸

$$R_{\text{cross}} = 2\delta + 2\gamma_\infty \left(\frac{\partial\delta}{\partial T} \right)_P \left(\frac{\partial T}{\partial\gamma_\infty} \right)_P. \quad (17)$$

The temperature derivatives in Eq. (17) are obtained by fitting the function

$$X = A + B(T - T_0) + CT \ln(T/T_0) \quad (18)$$

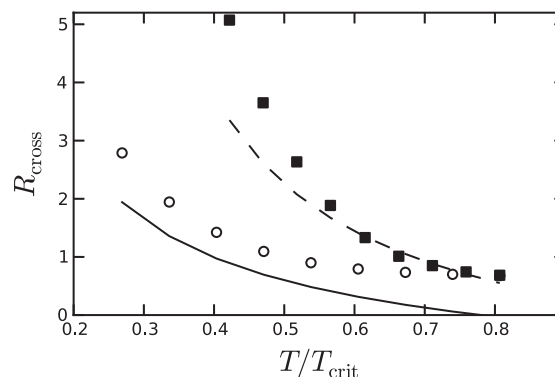


FIG. 8. Entropic sign crossover lengths (i.e., the cavity radius, in units of solvent diameters, at which the solvation entropy changes sign from negative to positive) plotted as a function of temperature reduced by T_{crit} , the liquid-vapor critical temperature. The open circles and filled squares are C-EoS predictions for the Jagla liquid and water, respectively. The solid and dashed lines are predictions for the Jagla liquid and water, respectively, using Eq. (17). Entropic crossovers for cavities in the LJ liquid also occur, but at cavity radii less than 0.5 solvent diameters for all states on the saturation curve (not shown).

for $X = \gamma_\infty$ and the combination of variables $\gamma_\infty\delta$. We note that Eq. (17) requires constant pressure temperature derivatives and we have used data along the saturation curve. However, the differences between the two paths are small at low pressures. For low temperature states, the predictions from Eq. (17) are qualitatively similar to those given by the C-EoS. Although the entropic crossover is similar in the Jagla liquid and water, the crossover in water is predicted by either scheme to occur for radii larger than the solvent diameter at essentially all liquid temperatures, in contrast to the Jagla liquid.

E. The thermodynamic stability of solvophobic aggregates

To explore the implications of the interplay between temperature and length scale dependence of solvation free energies, we examine a simple picture of solvophobic aggregation that combines ideas from classical homogeneous nucleation theory⁵³ and recent work from Chandler¹ and Rajamani *et al.*⁶ Consider a solvophobic aggregate composed of n identical hard sphere particles with cavity radius r such that the total volume of the aggregate is $V = nv/\eta$, where v is the volume of a single constituent hard sphere particle and η is the packing fraction of the spheres. If the aggregate is treated as a large spherical volume of radius R , then the aggregation Gibbs energy may be modeled as

$$\Delta G = \mu_R - n\mu_r, \quad (19)$$

where μ_R is the aggregate’s chemical potential and μ_r is the chemical potential of a single constituent solvophobe at infinite dilution. The relationship between the number of hard spheres comprising the aggregate and its radius, R , is $n = 4\pi\eta R^3/3v$. Combining the expressions for n and ΔG and dividing by the aggregate surface area, we have

$$\Delta G(R)/4\pi R^2 = \mu_R(R)/4\pi R^2 - \mu_r\eta R/3v. \quad (20)$$

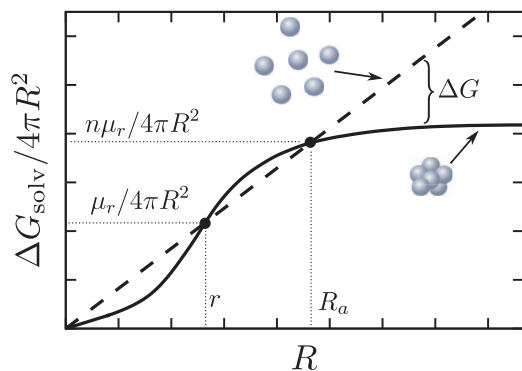


FIG. 9. Solvation free energy scaled by the surface area versus aggregate radius. The solid line corresponds to the solvation free energy per unit surface area of a cavity of size R , which is used to model an aggregate of n smaller hard spheres of size r (see text). The dashed line represents the solvation free energy per unit surface area for n constituent spheres fully dispersed in solution. Only aggregates larger than the aggregation radius, R_a , are thermodynamically stable.

For increasing R , the first term on the RHS of Eq. (20) becomes approximately constant and equal to the interfacial free energy per unit area.³ The second term is a linear function of the aggregate radius. The radius at which the RHS vanishes is the aggregation radius, R_a —aggregates of size larger than R_a are thermodynamically stable within this model free energy. These concepts are shown pictorially in Fig. 9.

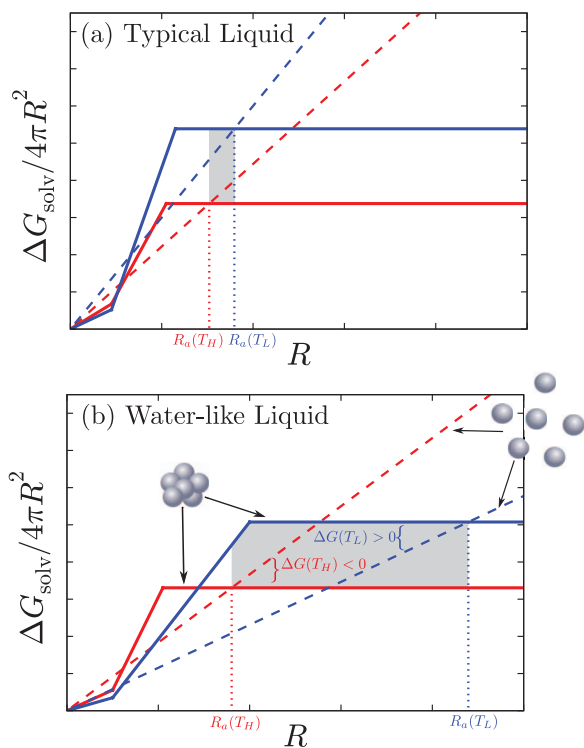


FIG. 10. Qualitative depiction of solvation free energy per surface area of large solvophobic aggregates and dispersed small solutes in (a) typical and (b) water-like solvents. Red and blue correspond to warm (T_H) and cold temperatures (T_L), respectively. The shaded region highlights the aggregate size range where cooling from T_H to T_L destabilizes the aggregate. The sloped line which here depicts the rise from very small solute to large radius behavior is used to emphasize that the shape of this molecular scale transition region is represented only generically in this figure.

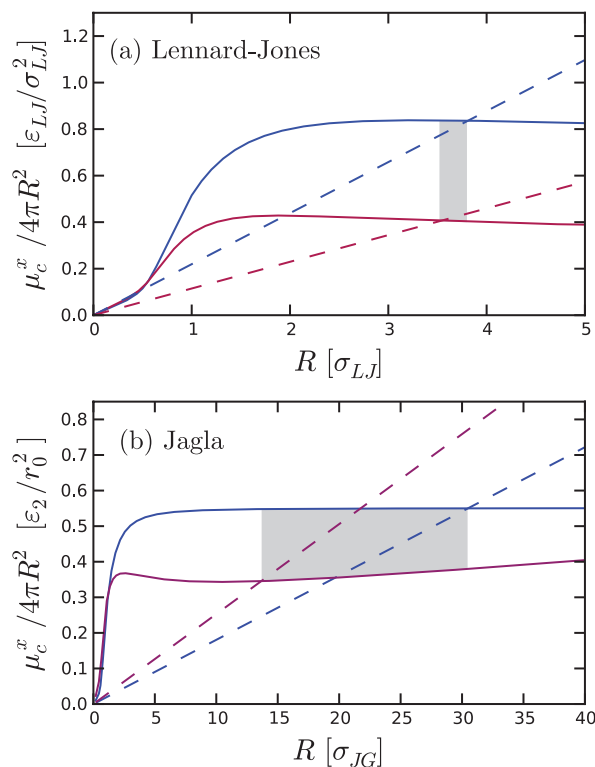


FIG. 11. The specific case of Fig. 10 for the temperature dependence of solvophobic solvation free energies in (a) the LJ liquid for $T = 0.65$ (blue) and $T = 0.95$ [ϵ_{LJ}/k_B] (red), and (b) the Jagla liquid for $T = 0.4$ (blue) and $T = 1.0$ [ϵ_2/k_B] (red). The constituent solvophobes are equivalent in size to the solvent diameter and the aggregate packing fraction is taken equivalent to the solvent packing fraction. Both liquids have a range of cavity sizes (shaded region) where cooling from the warm temperature (red lines) to the cool temperature (blue lines) destabilizes the aggregate (solid lines) relative to the dispersed spheres (dashed lines). The size range in the Jagla liquid is far more pronounced, however (note the order of magnitude difference in the abscissa scales).

We now consider the process of cooling the aggregate from a warm temperature, T_H , to a lower temperature, T_L , and in particular, the effect that this process has on the thermodynamic stability of the aggregate. A qualitative picture of the dependence of the aggregation radius, R_a , on temperature for a water-like and a reference LJ-like fluid is shown in Fig. 10. The differences in crossover behavior arise due to the fact that for small solutes in water-like solvents, increasing the temperature decreases the solubility. This has two effects: the first is that the crossover length scale is more sensitive to temperature, and the second is that the slope of the dispersed solvophobes line for high temperature is greater than the corresponding line at low temperature. These effects combine to produce a range of aggregate sizes that are thermodynamically stable at T_H but become unstable upon cooling to T_L . It is interesting that such a region also appears in a typical LJ-like liquid. However, the crossover length scale in LJ-like liquids is less sensitive to temperature and the slope of the dispersed solvophobes line is greater at lower temperatures, causing the region of destabilization to dramatically shrink or altogether disappear. Figure 11 shows quantitative measures of the dissociation size range in the LJ and Jagla liquids for cavities equivalent to the solvent size and aggregate packing

fractions equivalent to the solvent packing fraction. The dissociation region in the Jagla liquid is orders of magnitude larger than that in the LJ liquid.

In general, the range of the destabilization region is extended by cooling to lower temperatures or by composing aggregates of smaller constituent particles. A prediction made by this model is the possibility of cold-induced dissociation of solvophobic aggregates in LJ-like solvents. Aggregates composed of sufficiently small cavity solutes will in fact, in this model, have a range of sizes for which cooling will destabilize the aggregate and induce its decomposition. It would indeed be striking if such a limit were faithfully captured by this thought experiment in spite of its overall simplicity.

V. CONCLUSIONS

The results of exhaustive MC simulations of cavity formation along the saturation curves of the LJ liquid and the Jagla liquid were presented. The temperature-dependence of the solvation thermodynamics of cavities ranging from one-half to six times the solvent particle size were compared between the two simple liquids and to predictions for cavity formation in water given by a C-EoS. The comparisons between the Jagla liquid, water, and the simple liquid (LJ) serve to illuminate the features of hydrophobic hydration that are unique to water.

The Jagla liquid demonstrates water-like behavior in its resistance to dewetting of large cavity surfaces. In the presence of the largest cavity sizes considered (six solvent diameters), the LJ liquid showed a dewetting transition at all thermodynamic states on the saturation curve, whereas the Jagla liquid resists dewetting at low temperature saturation states.

The Jagla liquid is also water-like in its enthalpic and entropic behavior in the sense that the solvation entropy of small cavities is negative and the heat capacity increment is positive. The LJ liquid on the other hand manifests a strictly positive entropy for all cavities larger than half the solvent size and shows a negligible heat capacity increment.

From our analysis, we infer the important result that it is the existence of a second energy scale in the Jagla liquid and in water, compared to a simple liquid, that energetically favors the creation of void space at low temperatures, that gives rise to the anomalous liquid state properties as well as solvation behavior. Of course, the ability of the fluid to access the low energy structures with only modest expansion implies that the particular length scales involved are closely coupled to this observation.⁹

We have demonstrated that the scaling and temperature dependence of the solvation free energies of cavity solutes in Jagla liquid is qualitatively similar to that of water. Both liquids have negative solvation entropies for small cavities that cross over to positive with increasing cavity size. These crossovers for the Jagla liquid occur at a shorter length scale relative to the solvent size than those of water.

Combining ideas from Chandler¹ and Rajamani *et al.*,⁶ a simple model for aggregate dissociation was introduced by modeling an aggregate as a single large hard sphere with a volume equal to the sum of the volumes of the constituent spheres divided by a packing fraction. The consequences of

the differing size scaling and temperature dependence of solvation free energy for the aggregate compared to the dispersed constituent spheres is clearly demonstrated in the context of this simple model for aggregation. In particular, it was shown that cold-induced dissociation will occur for aggregates composed of sufficiently small spheres in water-like liquids. The degree to which such behavior is accurately described by the simple model is of interest for further investigations, as is the detailed examination of other two-scale liquids containing both a hard and soft core component.

ACKNOWLEDGMENTS

The authors are grateful to Henry S. Ashbaugh for providing us with the numerical results of his calculations on the Lennard-Jones fluid. This project was supported by the National Science Foundation (Grant No. CHE-0910615) with additional support from the R. A. Welch Foundation (F-0019). P.G.D. gratefully acknowledges the support of the National Science Foundation (Grant No. CHE-1213343). H.E.S. and S.V.B. thank the National Science Foundation Chemistry Division for support (Grant Nos. CHE-0908218 and CHE-1213217). Computations were performed at the Texas Advanced Computing Center.

¹D. Chandler, *Nature (London)* **437**, 640 (2005).

²K. Lum, D. Chandler, and J. D. Weeks, *J. Phys. Chem. B* **103**, 4570 (1999).

³D. M. Huang, P. L. Geissler, and D. Chandler, *J. Phys. Chem. B* **105**, 6704 (2001).

⁴D. M. Huang and D. Chandler, *J. Phys. Chem. B* **106**, 2047 (2002).

⁵D. M. Huang and D. Chandler, *Phys. Rev. E* **61**, 1501 (2000).

⁶S. Rajamani, T. M. Truskett, and S. Garde, *Proc. Natl. Acad. Sci. U.S.A.* **102**, 9475 (2005).

⁷A. J. Patel, P. Varilly, and D. Chandler, *J. Phys. Chem. B* **114**, 1632 (2010).

⁸Z. Yan, S. V. Buldyrev, N. Giovambattista, and H. E. Stanley, *Phys. Rev. Lett.* **95**, 130604 (2005).

⁹Z. Yan, S. V. Buldyrev, N. Giovambattista, P. G. Debenedetti, and H. E. Stanley, *Phys. Rev. E* **73**, 051204 (2006).

¹⁰S. V. Buldyrev, G. Malescio, C. A. Angell, N. Giovambattista, S. Prestipino, F. Saija, H. E. Stanley, and L. Xu, *J. Phys.: Condens. Matter* **21**, 504106 (2009).

¹¹E. A. Jagla, *Phys. Rev. E* **58**, 1478 (1998).

¹²E. A. Jagla, *J. Chem. Phys.* **111**, 8980 (1999).

¹³S. V. Buldyrev, P. Kumar, P. G. Debenedetti, P. J. Rossky, and H. E. Stanley, *Proc. Natl. Acad. Sci. U.S.A.* **104**, 20177 (2007).

¹⁴Z. Su, S. V. Buldyrev, P. G. Debenedetti, P. J. Rossky, and H. E. Stanley, *J. Chem. Phys.* **136**, 044511 (2012).

¹⁵S. V. Buldyrev, P. Kumar, S. Sastry, H. E. Stanley, and S. Weiner, *J. Phys.: Condens. Matter* **22**, 284109 (2010).

¹⁶M. Maiti, S. Weiner, S. V. Buldyrev, H. E. Stanley, and S. Sastry, *J. Chem. Phys.* **136**, 044512 (2012).

¹⁷V. Molinero and E. B. Moore, *J. Phys. Chem. B* **113**, 4008 (2009).

¹⁸E. B. Moore and V. Molinero, *J. Chem. Phys.* **132**, 244504 (2010).

¹⁹E. B. Moore and V. Molinero, *Nature (London)* **479**, 506 (2011).

²⁰B. Widom, *J. Chem. Phys.* **39**, 2808 (1963).

²¹B. Widom, *J. Phys. Chem.* **86**, 869 (1982).

²²D. Frenkel and B. Smit, *Understanding Molecular Simulation: From Algorithms to Applications* (Academic, 2001).

²³D. A. Kofke and P. T. Cummings, *Mol. Phys.* **92**, 973 (1997).

²⁴H. S. Ashbaugh and L. R. Pratt, *Rev. Mod. Phys.* **78**, 159 (2006).

²⁵H. S. Ashbaugh and L. R. Pratt, *J. Phys. Chem. B* **111**, 9330 (2007).

²⁶H. S. Ashbaugh, *J. Chem. Phys.* **130**, 204517 (2009).

²⁷H. Reiss, H. L. Frisch, and J. L. Lebowitz, *J. Chem. Phys.* **31**, 369 (1959).

²⁸F. H. Stillinger, *J. Solution Chem.* **2**, 141 (1973).

²⁹D. M. Tully-Smith and H. Reiss, *J. Chem. Phys.* **53**, 4015 (1970).

³⁰F. H. Stillinger and M. A. Cotter, *J. Chem. Phys.* **55**, 3449 (1971).

³¹D. Ben-Amotz, *J. Chem. Phys.* **123**, 184504 (2005).

- ³²J. R. Errington and P. G. Debenedetti, *Nature (London)* **409**, 318 (2001).
- ³³L. Xu, S. V. Buldyrev, C. A. Angell, and H. E. Stanley, *Phys. Rev. E* **74**, 031108 (2006).
- ³⁴J. G. Kirkwood and F. P. Buff, *J. Chem. Phys.* **17**, 338 (1949).
- ³⁵J. P. R. B. Walton, D. J. Tildesley, J. S. Rowlinson, and J. R. Henderson, *Mol. Phys.* **48**, 1357 (1983).
- ³⁶See supplementary material at <http://dx.doi.org/10.1063/1.4789981> for simulation details.
- ³⁷H. J. C. Berendsen, J. R. Grigera, and T. P. Straatsma, *J. Phys. Chem.* **91**, 6269 (1987).
- ³⁸H. J. C. Berendsen, D. Van Der Spoel, and R. van Drunen, *Comput. Phys. Commun.* **91**, 43 (1995).
- ³⁹D. Van Der Spoel, E. Lindahl, B. Hess, G. Groenhof, A. E. Mark, and H. J. C. Berendsen, *J. Comput. Chem.* **26**, 1701 (2005).
- ⁴⁰S. Miyamoto and P. A. Kollman, *J. Comput. Chem.* **13**, 952 (1992).
- ⁴¹G. Bussi, D. Donadio, and M. Parrinello, *J. Chem. Phys.* **126**, 014101 (2007).
- ⁴²U. Essmann, L. Perera, M. L. Berkowitz, T. Darden, H. Lee, and L. G. Pedersen, *J. Chem. Phys.* **103**, 8577 (1995).
- ⁴³E. Lomba, N. G. Almarza, C. Martin, and C. McBride, *J. Chem. Phys.* **126**, 244510 (2007).
- ⁴⁴K. Binder, *Phys. Rev. A* **25**, 1699 (1982).
- ⁴⁵R. C. Tolman, *J. Chem. Phys.* **17**, 333 (1949).
- ⁴⁶D. M. Huang and D. Chandler, *Proc. Natl. Acad. Sci. U.S.A.* **97**, 8324 (2000).
- ⁴⁷G. Graziano, *J. Phys. Chem. B* **110**, 11421 (2006).
- ⁴⁸H. S. Ashbaugh, *Chem. Phys. Lett.* **477**, 109 (2009).
- ⁴⁹F. Sedlmeier and R. R. Netz, *J. Chem. Phys.* **137**, 135102 (2012).
- ⁵⁰N. Muller, *Acc. Chem. Res.* **23**, 23 (1990).
- ⁵¹G. Graziano and B. Lee, *J. Phys. Chem. B* **109**, 8103 (2005).
- ⁵²S. Matysiak, P. G. Debenedetti, and P. J. Rossky, *J. Phys. Chem. B* **115**, 14859 (2011).
- ⁵³E. M. Lifshitz, L. P. Pitaevskii, and L. D. Landau, *Physical Kinetics* (Pergamon, Oxford, 1981), Vol. 10.
- ⁵⁴L. Reichl, *A Modern Course in Statistical Physics* (Wiley-Interscience, 1998).
- ⁵⁵The temperature derivatives are taken along the saturation curve, σ , and they may be related to their constant pressure counterparts through the state variable relation (Ref. 54)

$$\left(\frac{\partial\mu_c^x}{\partial T}\right)_\sigma = \left(\frac{\partial\mu_c^x}{\partial T}\right)_P + \left(\frac{\partial\mu_c^x}{\partial P}\right)_T \left(\frac{\partial P}{\partial T}\right)_\sigma.$$

Noting that $(\partial\mu_c^x/\partial P)_T = v_c^x$, where v_c^x is the excess partial molar volume, we may write

$$s_c^x|_\sigma = -\left(\frac{\partial\mu_c^x}{\partial T}\right)_\sigma = s_c^x|_P - v_c^x \left(\frac{\partial P}{\partial T}\right)_\sigma.$$

Similarly,

$$h_c^x|_\sigma = \left(\frac{\partial\beta\mu_c^x}{\partial\beta}\right)_\sigma = h_c^x|_P - T v_c^x \left(\frac{\partial P}{\partial T}\right)_\sigma.$$

The fundamental differences between the liquids considered here are seen in both the saturation and constant pressure quantities.